

Insights into Diffusion Mechanisms in P2 Layered Oxide Materials by First-Principles Calculations

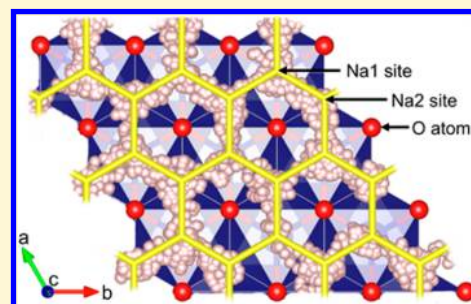
Yifei Mo,^{*,†,‡} Shyue Ping Ong,^{‡,§} and Gerbrand Ceder[‡]

[†]Department of Materials Science and Engineering, University of Maryland, College Park, Maryland 20742-2115, United States

[‡]Department of Materials Science and Engineering, Massachusetts Institute of Technology, Cambridge, Massachusetts 02139-4307, United States

[§]Department of NanoEngineering, University of California, San Diego, California 92093-0448, United States

ABSTRACT: Significant progress has been made in Na-intercalation compounds for rechargeable Na batteries. P2 Na_xMO_2 layered oxides have been shown to have high capacity, good cyclability, and improved rate capability. In this study, we investigate the diffusion mechanisms in P2 Na_xCoO_2 using *ab initio* molecular dynamics simulations and nudged elastic band calculations. We identify the Na diffusion mechanisms in P2 Na_xCoO_2 at nondilute Na concentrations and illustrate the strong effect of Na–Na interactions on Na diffusion. Our computational results demonstrate that P2 sodium layered oxides are fast Na ionic conductors over a wide range of Na concentrations and are promising cathode materials with high rate capabilities.



1. INTRODUCTION

Na-ion battery chemistry has recently experienced renewed interest as a potential energy storage alternative to Li-ion battery chemistry.^{1–5} Layered sodium transition metal oxides with the formula Na_xMO_2 ($M = \text{Co}, \text{Ni}, \text{Mn}, \text{Fe}, \text{V}, \text{Cr}, \text{etc.}$) have emerged as particularly promising compounds in terms of energy density and electrochemical performance.^{1–15} In contrast to layered Li_xMO_2 compounds, layered Na_xMO_2 materials can be synthesized in two different polymorphs, P2 and O3, where P (prismatic) and O (octahedral) denote the shape of the NaO_6 polyhedra and 2 and 3 denote the repetition unit perpendicular to the layers.^{16,17} Recent studies have suggested that P2 structures may in general outperform O3 structures in terms of reversible capacity. For example, Komaba and co-workers⁴ have demonstrated a reversible capacity of 190 mAh/g in P2 $\text{Na}_x(\text{Fe}_{1/2}\text{Mn}_{1/2})\text{O}_2$, and Lee et al.¹⁸ have shown a high rate capability in P2 $\text{Na}_x(\text{Ni}_{1/3}\text{Mn}_{2/3})\text{O}_2$.

Despite the apparent structural similarity, the Na diffusion topology in P2 Na_xMO_2 is manifestly distinct from the topology in O3. In P2, Na ions reside on two prismatic sites, Na1 and Na2. Na1 resides in an oxygen trigonal prism that is face-sharing with MO_6 octahedra above and below it, whereas the Na2 site prism is edge-sharing with MO_6 octahedra (Figure 1).¹⁶ First-principles calculations¹⁸ have suggested a low energy barrier of <0.2 eV for the migration of Na from the Na1 site to the Na2 site at Na concentrations from 0.33 to 0.67. The migration of Na between the two sites is likely to be affected by the interactions between Na ions. These interactions can be quite complex as distinctive Na orderings have been suggested at different Na concentrations.^{1,7,8,19–24} It is still not clear what the dominant Na migration mechanism is in P2 and how Na ordering affects the Na migration.

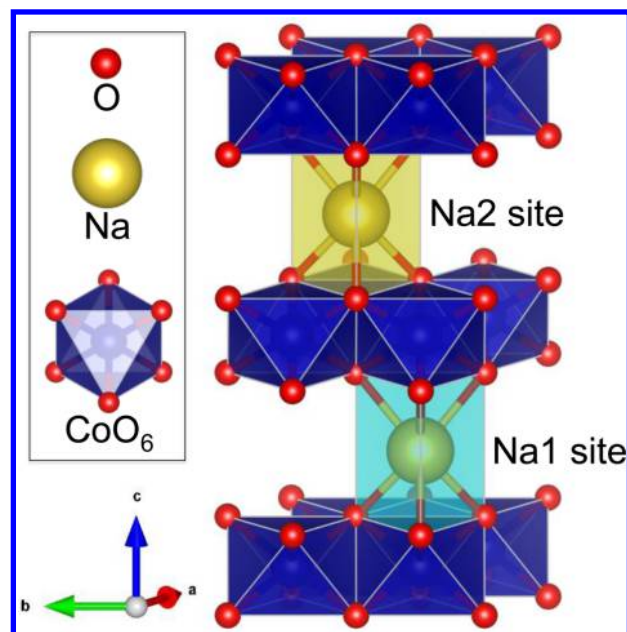


Figure 1. Crystal structure of P2 NaCoO_2 . The NaO_6 prims of the Na1 site (light green) and the Na2 site (yellow) share faces or edges with CoO_6 octahedra (blue), respectively. Both sites occur in each layer but are shown in separate layers for the sake of clarity.

In this paper, we present a comparative first-principles study of the diffusivity and diffusion mechanisms in P2 and O3 Na_xCoO_2 . Our results show that P2 Na_xCoO_2 has high Na

Received: April 30, 2014

Revised: July 29, 2014

Published: August 29, 2014

conductivity over a wide range of Na concentrations. We identify the Na diffusion mechanisms in P2 at nondilute Na concentrations and illustrate the strong effect of Na–Na interactions on Na diffusion. Our results show that Na diffusion in P2 is highly dependent on the local environment of the configurations of Na ions.

2. CALCULATION METHODS

All calculations were performed using the Vienna *ab initio* simulation package (VASP)²⁵ within the projector augmented-wave approach²⁶ using the Perdew–Burke–Ernzerhof generalized-gradient approximation (GGA)²⁷ to density functional theory. Because of the large unit cells, γ -point only sampling of k -space was used, and the plane-wave energy cutoff was set to 520 eV. The calculations were spin-polarized for relaxations and for nudged elastic band (NEB) calculations. For *ab initio* molecular dynamics (AIMD) simulations, non-spin-polarized calculations were performed with a lower plane-wave energy cutoff of 400 eV.

The supercell used for the O3 structure comprises $3 \times 3 \times 1$ conventional unit cells and 27 formula units, and the supercell for the P2 structure comprises $4 \times 4 \times 1$ conventional unit cells and 32 formula units. To model compounds at different Na concentrations (x), a fraction $(1 - x)$ of Na atoms was removed from each Na layer in the supercell. We investigated O3 supercells of 15, 18, and 21 Na atoms, which correspond to $x = 0.56, 0.67$, and 0.78 , respectively, and P2 supercells of 18, 22, and 24 Na atoms, which correspond to $x = 0.56, 0.69$, and 0.75 , respectively.

AIMD simulations were performed at 600, 720, 900, 1200, and 1500 K with a time step of 2 fs. All samples were heated to the desired temperature by velocity scaling at a rate of 500 K/ps. After the desired temperature had been reached, MD simulations in the NVT ensemble with a Nose-Hoover thermostat were performed. Samples were equilibrated for 40 ps before diffusion properties were measured. The movement of Na ions was monitored during the MD simulations, and the diffusivity of the Na ions was calculated on the basis of the Einstein relationship as described in our previous papers.^{28,29} For most data points, a total mean-square displacement of 2500–5500 Å² and a few thousand distinctive Na hops (~50–100 hops for each Na atom on average) accounted for the estimation of Na-ion diffusivity and conductivity. We excluded the data points that cannot reach this level of convergence during the MD simulations, such as O3 at 600 K. In addition, the data points of O3 at 1500 K were excluded because of the melting of the crystal structure.

The NEB method³⁰ was employed to calculate the energy barrier for Na migration. Full relaxations were performed on the supercell models at the initial and final states, which were extracted from AIMD simulations or constructed by removing Na atoms from the supercells. The initial migration path was constructed with seven linearly interpolated images between the starting and ending points. The energy barrier for migration was calculated as

$$\Delta E_a = E_{\max} - E_{\text{initial}}$$

where E_{\max} is the maximal energy during the migration path and E_{initial} is the energy at the initial state.³¹

3. RESULTS AND DISCUSSION

3.1. Na Diffusivity and Conductivity in Na_xCoO₂. Figure 2 and Table 1 show the diffusivities as obtained via MD simulations and the activation energies obtained either from MD at various temperatures or from NEB calculations. At low temperatures and/or high Na concentrations, the Na diffusion is too slow to be observed in MD simulations. For these concentrations, the activation energy is obtained from NEB calculations. The MD simulations show that partially desodiated P2 Na_xCoO₂ is a fast Na ionic conductor (Figure 2 and Table 1). The Na ionic conductivity extrapolated to 300 K is as high as 4 and 6 mS/cm for P2 Na_xCoO₂ at $x = 0.56$ and

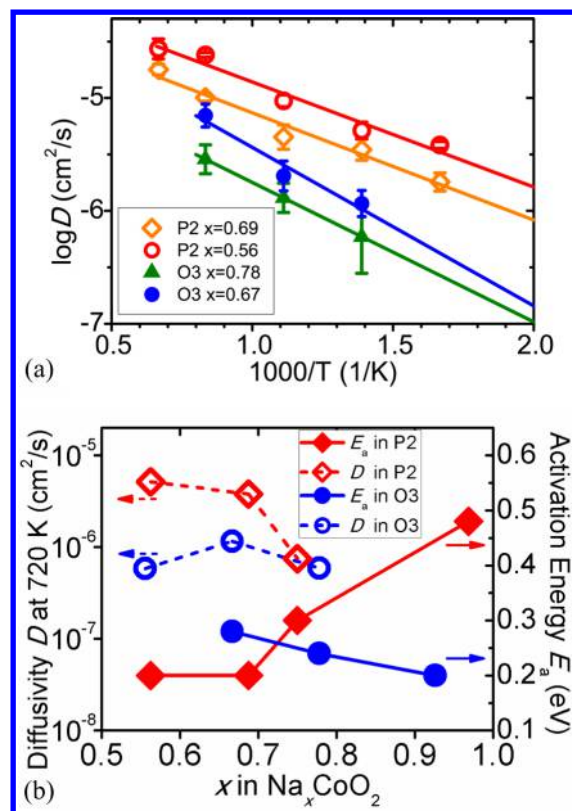


Figure 2. (a) Arrhenius plot of Na diffusivity in P2 and O3 Na_xCoO₂. Compared to those of the P2 structures, the O3 structures have lower diffusivities and higher activation energies. (b) Activation energy E_a and diffusivity at 720 K as a function of Na concentration x in P2 and O3 Na_xCoO₂.

Table 1. Activation Energies and Ionic Conductivities of P2 and O3 Na_xCoO₂ at Different Na Concentrations (x)

	x in Na _x CoO ₂	activation energy (eV)	ionic conductivity extrapolated to 300 K (mS/cm)	calculation method
O3	single divacancy (25/27)	0.20	–	NEB
	0.78 (21/27)	0.24	0.3	AIMD
	0.67 (18/27)	0.28	0.1	AIMD
	0.56 (15/27)	Na diffusivity is $1/3$ of that at $x = 0.67$ at 720 K ^a		AIMD
P2	single vacancy (31/32)	0.48	– ^a	NEB
	0.75 (24/32)	0.30	0.1	AIMD
	0.69 (22/32)	0.20	4	AIMD
	0.56 (18/32)	0.20	6	AIMD

^aDiffusion is too slow in AIMD to obtain statistically converged results.

0.69, respectively. These conductivities and activation energies are comparable to those found in some of the best Li-ion conductors.²⁸ The activation energy for Na ionic diffusion is as low as 0.20 eV at both Na concentrations. The O3 structured Na_xCoO₂ also has good diffusivity. The activation energy of O3 at $x = 0.67$ and 0.78 ranges from 0.24 to 0.28 eV, and the ionic conductivity extrapolated to 300 K ranges from 0.1 to 0.3 mS/cm, which is 1 order of magnitude lower than that of P2 (Table 1).

How Na conductivity changes with Na concentration is of interest in understanding the charging–discharging behavior in Na-ion batteries. In our simulations, Na conductivity in O3 decreases as x approaches 0.5 (Table 1). This decrease for x values near 0.5 is likely caused by the ordering of Na ions at $x = 0.5$. We also expect a decrease in Na conductivity at x values near 1 as a result of the depletion of divacancies. This concentration dependence is consistent with previous results of Li diffusion in O3 Li_xCoO_2 .³¹

In contrast, the Na conductivity in P2 increases monotonically as Na content x decreases (Table 1 and Figure 2). At high Na concentrations ($x > 0.75$), Na diffusion in P2 is slower than in O3. For example, at $x \sim 0.75$, Na diffusion in P2 has an activation energy of 0.3 eV, which is higher than the activation energy of 0.24 eV in O3. This is consistent with different transport mechanisms for P2 and O3 at low vacancy concentrations. The energy barrier for a single-vacancy migration in P2 is 0.48 eV at the dilute limit $x \sim 1$ (see section 3.2), while the energy barrier for an isolated divacancy in O3 is as low as 0.2 eV.³ On the other hand, Na conductivity in P2 increases as x approaches 0.5 in contrast to the decrease in conductivity observed in O3. The extrapolated Na conductivity at 300 K is as high as 6 mS/cm at $x = 0.5$, which is 1–2 orders of magnitude higher than the diffusion in O3 at the same concentration. This concentration dependence is consistent with experimental results for Na_xCoO_2 .³² We analyze the Na hops and trajectories in our AIMD simulations to shed light on the difference in the concentration dependence of the diffusivity between P2 and O3 structures.

3.2. Single-Vacancy Migration in P2. The activation barrier for a single-vacancy migration in P2 is evaluated by the NEB method. The lowest-energy migration path is illustrated in Figure 3, and the energy barrier for the single-vacancy

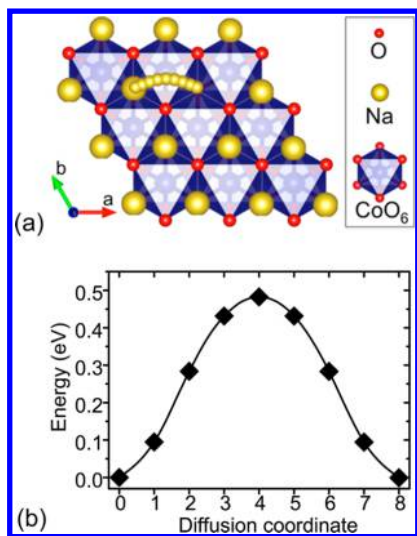


Figure 3. Single-vacancy hopping in P2: (a) lowest-energy migration path (small yellow spheres) in the NEB calculation and (b) energy along the migration path.

migration is 0.48 eV, which is significantly higher than the activation energies at lower Na concentrations in MD simulations (Table 1 and Figure 2). The energy barrier obtained from the NEB method is consistent with the experimental value of ~ 0.5 eV in Na_xCoO_2 at a Na concentration $x > 0.85$.³² The high migration energy barrier is caused by the strong electrostatic repulsion between the Na

ions on the nearest-neighbor Na1 and Na2 sites at the activated state of the vacancy migration.

3.3. Divacancy Mechanism Not Active in P2. Previous work by Van der Ven et al. has shown that the diffusion of Li ions in O3 structures of Li_xCoO_2 is mediated by divacancies, whereby Li ion migrates through a tetrahedral LiO_4 site into one vacant site of the divacancies.³¹ Ong et al.³ have confirmed the migration barrier to be as low as 0.18 eV for an isolated divacancy in O3 Na_xCoO_2 . From the AIMD simulations, we confirm that the divacancy migration is indeed the dominant mechanism for Na diffusion in O3 at all concentrations.

To test whether the divacancy mechanism is active in P2, a MD simulation was performed on a supercell with one divacancy, i.e., two unoccupied Na2 sites, in each Na layer (Figure 4a). There was no continuous hopping of Na ions

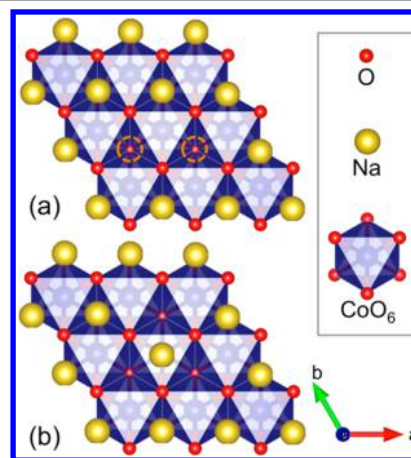


Figure 4. (a) Divacancy that consists of two vacancies (orange spheres) on the Na2 sites in P2. (b) Structure after the relaxation of a divacancy.

during the MD simulation. Instead, we observe in the MD simulation that a Na ion on a Na2 site adjacent to the divacancy migrated into the Na1 site (Figure 4) between the two vacancies. This migration formed a new Na local configuration, which was comprised of a Na ion on the Na1 site with three unoccupied Na2 sites as nearest neighbors (Figure 4b). This observation is confirmed by DFT relaxation calculations, which show the same spontaneous migration of Na2 into Na1. Therefore, an isolated divacancy is not a stable defect in P2, and the divacancy mechanism is not active in P2 because of the absence of these divacancy defects. The ability for Na to occupy the Na1 site effectively destroys the divacancies, leading to more difficult Na diffusion at high concentrations in P2.

3.4. Na Diffusion Pathways in P2. The lack of a divacancy mechanism suggests that Na diffusion in P2 is different from that in O3. This difference is caused by the existence of a wide range of local Na configurations consisting of occupied and unoccupied Na1 and Na2 sites. The trace of Na movements in the MD simulations (Figure 5) reveals that Na ions always migrate between Na1 and Na2 sites. Therefore, the P2 diffusion topology is a two-dimensional honeycomb lattice of interconnected Na sites, in which Na1 and Na2 sites alternate. We also find in the MD simulations that nearest-neighbor Na1 and Na2 sites are never occupied at the same time, which is likely due to strong electrostatic repulsion between nearest-neighbor Na1 and Na2 ions that are only ~ 1.6 Å apart and is consistent

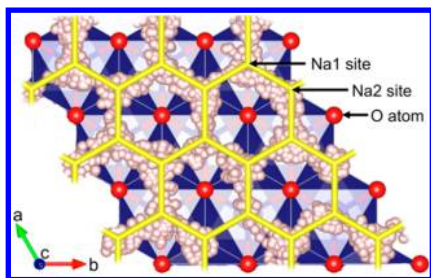


Figure 5. Pathway of Na migration in P2 $\text{Na}_{0.56}\text{CoO}_2$. The white spheres indicate the trace of Na positions during MD simulations, and yellow lines highlight the diffusion pathways.

with previous reports.^{20,21} We now investigate further how Na moves in this honeycomb sublattice.

3.5. Diffusion Mechanism: How Na Ions Hop in P2. To understand the local Na configurations at the time of a Na hop, we examined the environment around all Na hops in the MD simulations. Examples of hopping events are shown in panels a and b of Figure 6. The Na coordination number of the hopping Na ion changes before and after the hopping. For example, as a result of the hop in Figure 6a, the Na ion gains two second nearest-neighbor Na ions and loses four third nearest-neighbor Na ions. To facilitate the analysis of the Na hops, we establish the following formalism to characterize local Na configurations using Na–Na coordination numbers.

(1) We define the Na–Na coordination numbers, c_2 and c_3 , as the number of Na atoms on the second-nearest-neighbor and third-nearest-neighbor sites, respectively (the first nearest neighbor is always unoccupied, i.e., $c_1 = 0$). For each Na in the Na1 or Na2 site, there are six second-nearest-neighbor sites and nine third-nearest-neighbor sites, and the values of c_2 and c_3 range from 0 to 6 and from 0 to 9, respectively.

(2) We define a hop as the migration of a Na ion from a Na1 site to its nearest-neighbor Na2 site or vice versa. Because Na ions are constantly moving in MD simulations, the occupancy of a site is considered valid if the site has been occupied for more than 2 ps.

(3) We classify each Na hop as $(\Delta c_2, \Delta c_3)$, where Δc is the change in coordination number upon hopping. For example, the hop in Figure 6a is denoted as $(+2, -4)$ as the Na ion gains two second nearest neighbors and loses four third nearest neighbors.

On the basis of this formalism, a statistical analysis was performed for all Na hops that occurred during the MD simulations, and the fraction of each hop, $(\Delta c_2, \Delta c_3)$, is represented in Figure 7a. We may observe that there are four dominant peaks with the highest fraction (red rectangles in Figure 7a), which are $(-2, +4)$, $(+2, -4)$, $(-1, +2)$, and $(+1, -2)$; hops with other values of $(\Delta c_2, \Delta c_3)$ occur at a much lower frequency. Examples of the local Na configurations for these dominant hops, such as $(+2, -4)$ and $(+1, -2)$, are illustrated in panels a and b of Figure 6, respectively. The $(+2, -4)$ hop in Figure 6a has an initial state of no second nearest neighbor and four third nearest neighbors and a final state of two second nearest neighbors ($\Delta c_2 = +2$) and no third nearest neighbor ($\Delta c_3 = -4$). For the $(+1, -2)$ hop in Figure 6b, the second nearest neighbor increases from 1 to 2 ($\Delta c_2 = +1$) and the third nearest neighbor decreases from 4 to 2 ($\Delta c_3 = -2$).

To understand the dependence of the migration energy barrier on the local Na configuration, NEB calculations are performed on all hops observed in the MD simulations. Combining these activation energies with the statistical results from the MD simulations, we plot the fractional distribution of hops as a function of activation energy in panels b and c of Figure 7. The peak at 0.16–0.20 eV corresponds to mostly $(+2, -4)$ hops and similar hops such as $(+2, -3)$ and $(+2, -5)$ (red bars in Figure 7b). Other dominant types of hops have much lower activation energies for migration. For example, the $(-1, +2)$ and $(+1, -2)$ hops most frequently occur at 0.10–0.12 eV (Figure 7c), and the $(-2, +4)$ hops have an activation energy of <0.04 eV (Figure 7b). Among all these different type of hops, the $(+2, -4)$ hops have the highest activation energies, which agrees with the activation energy observed in MD simulations (Table 1). Therefore, the $(+2, -4)$ hops are likely the rate-limiting steps for Na migration in P2. One such $(+2, -4)$ hop is illustrated in Figure 6a, and its corresponding migration energy

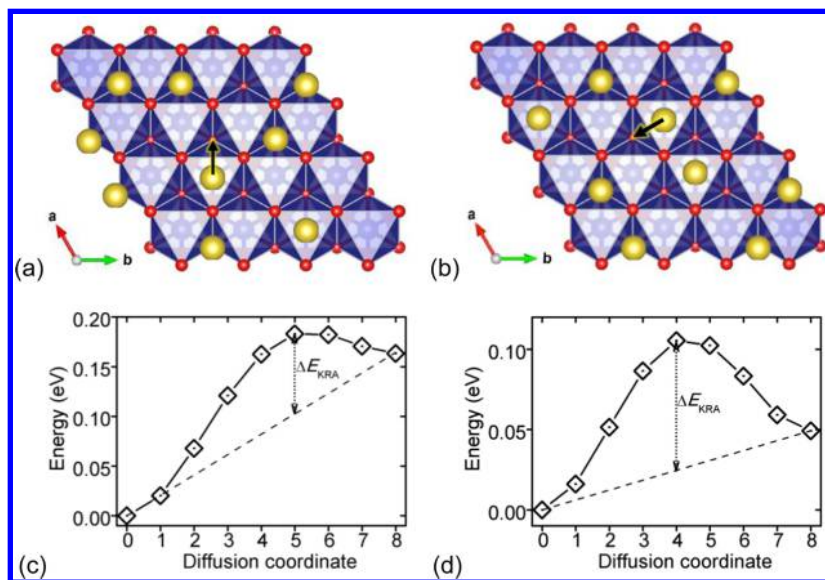


Figure 6. Hops observed in the MD simulations. The hops in panels a and b are classified as $(+2, -4)$ and $(+1, -2)$, respectively, by the change in Na coordination. The corresponding migration energy barriers of the hops in panels a and b are shown in panels c and d, respectively.

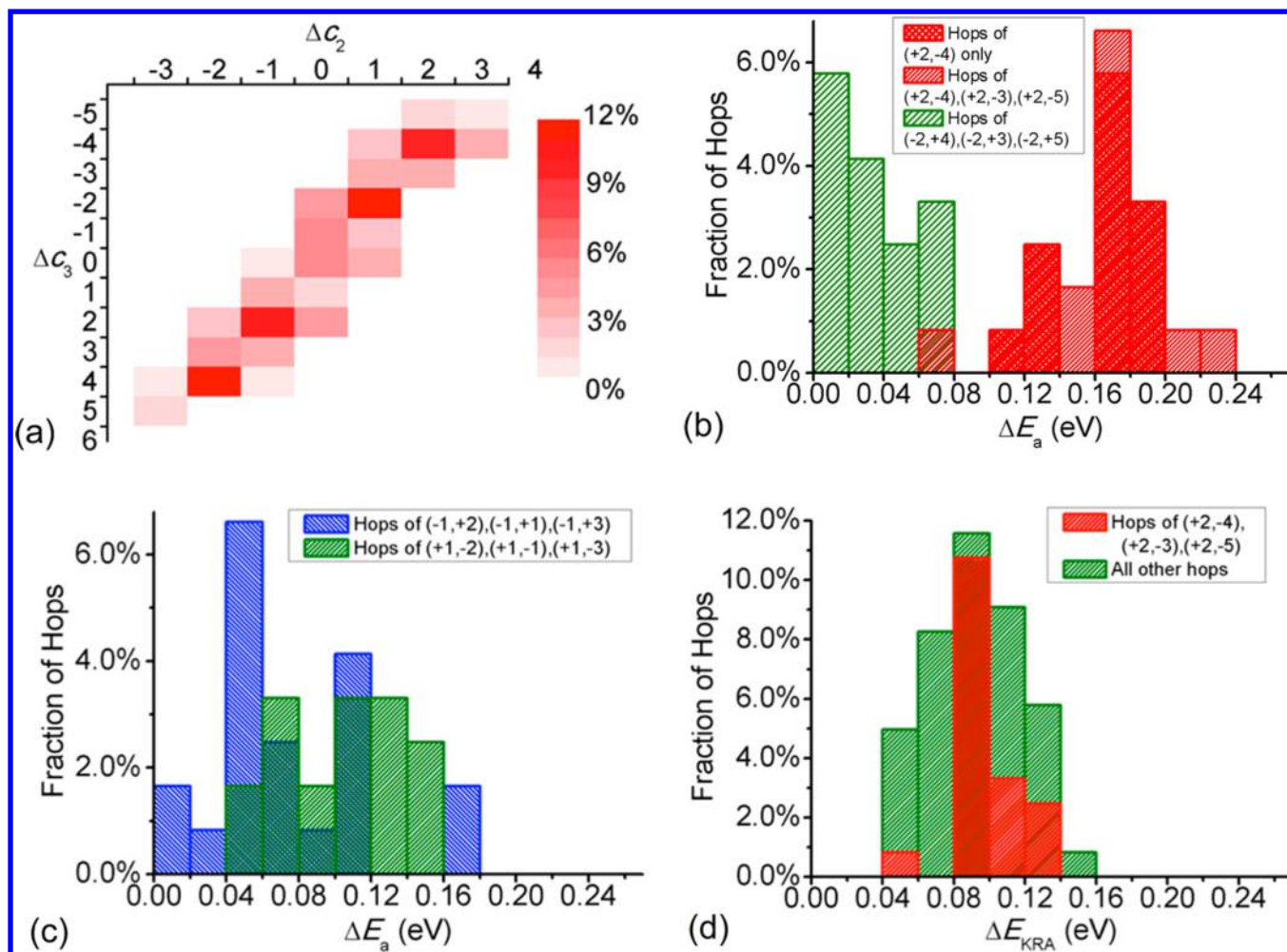


Figure 7. (a) Fraction of each Na hop, $(\Delta c_2, \Delta c_3)$, extracted from an AIMD simulation for 160 ps in P2 $\text{Na}_{0.56}\text{CoO}_2$ at 600 K. (b and c) Fraction of each hop separated by the activation barrier ΔE_a with which they occur. (d) Kinetically resolved activation barriers ΔE_{KRA} during the same MD simulation.

barrier is 0.19 eV. The energy along its diffusion path (Figure 6c) shows that a significant fraction of the activation energy can be ascribed to the increase in energy in going from the initial to the final Na site.

To exclude the effect of the energy difference between the final and initial states of Na hopping, we apply the concept of the kinetically resolved activation (KRA) energy barrier^{31,33}

$$\Delta E_{KRA} = \Delta E_a - (E_{\text{final}} - E_{\text{initial}})/2$$

where E_{final} (E_{initial}) is the energy at the final (initial) state of Na hopping. The advantage of defining ΔE_{KRA} is that it is identical for the forward and backward hop. The fraction of hops with different values of ΔE_{KRA} is shown as a histogram in Figure 7d. There is a single peak at 0.10 eV for different type of hops, and ΔE_{KRA} ranges from 0.04 to 0.14 eV. The (+2,-4) hops have KRA barriers similar to those of other types of hops. This result suggests that the energy barrier for migration of Na from the Na1 site to the Na2 site is intrinsically low. The higher activation energy observed for some hops [such as (+2,-4) hops] is due to an extra energy increase from the initial state to the final state of Na hopping. This energy increase is like due to the electrostatic repulsion among Na ions. For example, the system energy increases when the number of second nearest neighbors increases as in the (+2,-4) hops.

3.6. Implications for Na-Ion Batteries. Our results provide a better understanding of the Na diffusion mechanism in P2. Na ions migrate through a honeycomb sublattice in the P2 Na layer (Figure 5), which is distinctive from the triangular Na sublattice in the O3 Na layers. This honeycomb lattice has a low intrinsic energy barrier of approximately 0.1 eV for Na migration. This energy barrier may increase significantly by the strong repulsive electrostatic interactions among Na ions. These Na–Na interactions are likely the main limiting factor for Na diffusion in P2. For example, the activation energy barrier increases to ~ 0.2 eV for certain types of Na hops at $x = 0.56$ and 0.68. These particular hops with higher activation energies are essential for forming the percolation diffusion pathway and therefore control the overall activation energy barrier for Na diffusion as observed in MD simulations.

Fast Na diffusion can occur if a percolating path with low migration energy barriers exists. At high Na concentrations, the probability of low-migration energy hops in the P2 topology is low, and the hops with high energy barriers can be avoided in the formation of Na percolation paths. Take, for instance, the limiting case of a single vacancy in a P2 layer, with all Na in the Na2 sites. The migration event of a single vacancy is a Na^+ hop from the Na2 site to a transition state Na1 site followed by a hop into the vacant site as illustrated in section 3.2 (Figure 3). The transition state where the Na is in the Na1 site is high in

energy ($E_a = 0.48$ eV for single-vacancy migration), given that this Na1 site experiences strong electrostatic repulsion from the Na⁺ in the adjacent Na2 site that is only ~ 1.6 Å away (Figure 3). This leads to high migration energy barriers. Therefore, we explain the sluggish Na diffusion at high Na concentrations in P2 by the strong electrostatic interactions among Na ions. This slow Na diffusion at high Na concentrations may partly account for the poor cyclability of P2 at $x > 0.90$.^{1,32}

Given the strong effect of Na–Na interactions on the local Na migration energy, Na diffusion is substantially affected by Na ordering. Experimental and computational studies have shown pronounced Na ordering in P2.^{1,7,8,19–22,24} We expect the Na diffusivity to decrease when Na ordering forms. This decrease in diffusivity due to lattice ordering has been shown in previous first-principles modeling for Li diffusion in O3 Li_xCoO₂.³¹ Na ordering and Na diffusion are also influenced by the sublattice of transition metal cations Co³⁺ and Co⁴⁺. For example, the Na2 site is usually preferred over the Na1 site at high Na concentrations as the latter site face-shares with the octahedron around Co cations. At lower Na concentrations, the ability to weaken Na–Na repulsion results in the occupancy of both the Na1 and Na2 sites.^{20,21} Mixing distinct transition metal elements may perturb the ordering of the transition metal sublattice and result in a weaker Na ordering, which improves the Na diffusion in P2. Therefore, designing multi-transition metal oxides in P2 may be a path toward a good rate across a large capacity range, as evidenced by the excellent performance of some mixed transition metal P2 compounds.^{4,8,9,11,12,18}

The O3 structure does not suffer from low Na diffusion at high Na concentrations, because divacancies mediate the diffusion over the whole range of Na concentrations.³¹ The drawback of O3 is the drop in diffusion at $x \sim 0.5$. In comparison, P2 is a fast ionic conductor at $x \sim 0.5$ and is expected to remain so for $x < 0.5$. The fast Na conduction at $x \sim 0.5$ may partly explain why P2 can be cycled to the lower half of Na concentrations ($x < 0.5$) in some experimental studies.^{1,18} In addition, in the medium range of Na concentration, e.g., $0.5 < x < 0.75$ and possibly $x < 0.5$, P2 outperforms O3 significantly in terms of Na conductivity. P2 may be suitable for high rate application if the cycling is limited within the Na concentration window with high conductivity.

4. CONCLUSIONS

First-principles studies were performed to assess Na diffusion mechanisms in P2 sodium layered oxide materials. Our results indicate that both P2 and O3 show good Na conductivities over a wide range of Na concentrations. P2 outperforms O3 for Na conductivity except at high Na concentrations. Our calculations determined that Na diffusion in P2 is not mediated by divacancies, which is the dominant carrier for Na diffusion in O3. Instead, Na ions migrate with a low energy barrier in a honeycomb sublattice in P2. The strong electrostatic interactions among Na ions and Na ordering are the major limiting factor for Na migration in P2 and are particularly problematic at high Na concentrations. Our results show that P2-type layer oxide materials are promising cathode materials with good rate capabilities for Na-ion batteries.

AUTHOR INFORMATION

Corresponding Author

*E-mail: yfmo@umd.edu.

Notes

The authors declare no competing financial interest.

ACKNOWLEDGMENTS

This work was partially supported by the U.S. Department of Energy (DOE) under Contract No. DE-FG02-96ER45571. This research used computational resources from the Extreme Science and Engineering Discovery Environment (XSEDE), which was supported by National Science Foundation grant number TG-DMR970008S and TG-DMR130142. Y. Mo thanks the funding support from the Minta Martin award and the University of Maryland supercomputing resources (<http://www.it.umd.edu/hpcc>).

REFERENCES

- Berthelot, R.; Carlier, D.; Delmas, C. *Nat. Mater.* **2011**, *10*, 74.
- Kim, S.; Ma, X.; Ong, S. P.; Ceder, G. *Phys. Chem. Chem. Phys.* **2012**, *14*, 15571.
- Ong, S. P.; Chevrier, V. L.; Hautier, G.; Jain, A.; Moore, C.; Kim, S.; Ma, X.; Ceder, G. *Energy Environ. Sci.* **2011**, *4*, 3680.
- Yabuuchi, N.; Kajiyama, M.; Iwatate, J.; Nishikawa, H.; Hitomi, S.; Okuyama, R.; Usui, R.; Yamada, Y.; Komaba, S. *Nat. Mater.* **2012**, *11*, 512.
- Slater, M. D.; Kim, D.; Lee, E.; Johnson, C. S. *Adv. Funct. Mater.* **2013**, *23*, 947.
- Kim, S.-W.; Seo, D.-H.; Ma, X.; Ceder, G.; Kang, K. *Adv. Energy Mater.* **2012**, *2*, 710.
- Caballero, A.; Hernan, L.; Morales, J.; Sanchez, L.; Santos Pena, J.; Aranda, M. A. G. *J. Mater. Chem.* **2002**, *12*, 1142.
- Lu, Z.; Dahn, J. R. *J. Electrochem. Soc.* **2001**, *148*, A1225.
- Carlier, D.; Cheng, J. H.; Berthelot, R.; Guignard, M.; Yoncheva, M.; Stoyanova, R.; Hwang, B. J.; Delmas, C. *Dalton Trans.* **2011**, *40*, 9306.
- Bhide, A.; Hariharan, K. *Solid State Ionics* **2011**, *192*, 360.
- Wang, X.; Tamaru, M.; Okubo, M.; Yamada, A. *J. Phys. Chem. C* **2013**, *117*, 15545.
- Buchholz, D.; Chagas, L. G.; Winter, M.; Passerini, S. *Electrochim. Acta* **2013**, *110*, 208.
- Ding, J. J.; Zhou, Y. N.; Sun, Q.; Yu, X. Q.; Yang, X. Q.; Fu, Z. W. *Electrochim. Acta* **2013**, *87*, 388.
- Shimono, T.; Tanabe, D.; Kobayashi, W.; Moritomo, Y. *J. Phys. Soc. Jpn.* **2013**, *82*, 083601.
- Kim, D.; Kang, S.-H.; Slater, M.; Rood, S.; Vaughey, J. T.; Karan, N.; Balasubramanian, M.; Johnson, C. S. *Adv. Energy Mater.* **2011**, *1*, 333.
- Delmas, C.; Fouassier, C.; Hagenmuller, P. *Physica B+C (Amsterdam)* **1980**, *99*, 81.
- Delmas, C.; Braconnier, J.-J.; Fouassier, C.; Hagenmuller, P. *Solid State Ionics* **1981**, *3–4*, 165.
- Lee, D. H.; Xu, J.; Meng, Y. S. *Phys. Chem. Chem. Phys.* **2013**, *15*, 3304.
- Shu, G. J.; Chou, F. C. *Phys. Rev. B* **2008**, *78*, 052101.
- Hinuma, Y.; Meng, Y.; Ceder, G. *Phys. Rev. B* **2008**, *77*, 224111.
- Meng, Y. S.; Hinuma, Y.; Ceder, G. *J. Chem. Phys.* **2008**, *128*, 104708.
- Zhang, P.; Capaz, R. B.; Cohen, M. L.; Louie, S. G. *Phys. Rev. B* **2005**, *71*, 153102.
- Tanabe, D.; Shimono, T.; Kobayashi, W.; Moritomo, Y. *Phys. Status Solidi RRL* **2013**, *7*, 1097.
- Meng, Y. S.; Van der Ven, A.; Chan, M. K. Y.; Ceder, G. *Phys. Rev. B* **2005**, *72*, 172103.
- Kresse, G.; Furthmüller, J. *Phys. Rev. B* **1996**, *54*, 11169.
- Blöchl, P. E. *Phys. Rev. B* **1994**, *50*, 17953.
- Perdew, J. P.; Ernzerhof, M.; Burke, K. *J. Chem. Phys.* **1996**, *105*, 9982.
- Mo, Y.; Ong, S. P.; Ceder, G. *Chem. Mater.* **2012**, *24*, 15.

- (29) Ong, S. P.; Mo, Y.; Richards, W. D.; Miara, L.; Lee, H. S.; Ceder, G. *Energy Environ. Sci.* **2013**, *6*, 148.
- (30) Mills, G.; Jónsson, H.; Schenter, G. K. *Surf. Sci.* **1995**, *324*, 305.
- (31) Van der Ven, A.; Ceder, G.; Asta, M.; Tepeš, P. *Phys. Rev. B* **2001**, *64*, 184307.
- (32) Takayuki, S.; Wataru, K.; Yutaka, M. *Appl. Phys. Express* **2013**, *6*, 097101.
- (33) Bhattacharya, J.; Van der Ven, A. *Phys. Rev. B* **2010**, *81*, 104304.